J. Materials, Conc. Struct. Pavements, JSCE, No. 704/V-55, 271-280, 2002 May

BEM ANALYSIS OF MIXED-MODE CRACK PROPAGATION DUE TO CORROSION OF REINFORCEMENT IN CONCRETE

Farid UDDIN A.K.M.[1] and Masayasu OHTSU[2]

[1]Student Member of JSCE, Graduate Student, Graduate School of Science and Technology, Kumamoto University (Kurokami 2-39-1, Kumamoto 860-8555, Japan)

[2]Member of JSCE, Dr. of Eng., Professor, Graduate School of Science and Technology, Kumamoto University (Kurokami 2-39-1, Kumamoto 860-8555, Japan)

Due to expansion of corrosive products, cracks are nucleated around reinforcement in concrete. Initiation and propagation of these cracks are studied by experimentally and then analytically by the Boundary Element Method (BEM). The maximum circumferential stress criterion is applied to trace the crack extension of mixed-mode cracking. By employing the two-domain BEM, crack orientations are evaluated from the stress intensity factors of mode I and mode II. In BEM analysis, the ratios of stress intensity factors of mode I to mode II (K_I/K_{II}) are studied for the different types of crack patterns, which are observed as corrosion cracking.

Key Words: *linear elastic fracture mechanics, stress intensity factors, mixed-mode cracking, corrosion*

1. INTRODUCTION

Corrosion is a subsidiary problem of reinforced concrete (RC) structures, which are subjected to severe salt attack. It is known as one of the major deterioration mechanisms in RC structures. Because concrete is a porous material, carbon dioxide and chloride can easily penetrate into it. As a result, the passivity of the steel is destroyed, and then the reinforcement (rebar) in concrete is corroded. The expansion of corrosion products generates cracks which result in serious defects in RC structures. When the rebar is corroded, corrosion products expand the area of the reinforcement and generate tensile stress around it. Since concrete can endure less tensile stress than compressive stress, tensile cracks are readily nucleated and propagate in concrete. Due to corrosion of the rebar, cracks are observed in a variety of patterns. These are reported to be related with cover thickness, concrete properties and arrangement of reinforcement[1].

The maximum circumferential stress criterion based on linear elastic fracture mechanics (LEFM) was successfully applied to trace the crack extension of mixed-mode cracking[2]. By employing the two-domain Boundary Element Method (BEM), crack orientations were evaluated from the stress intensity factors of mode I and mode II. The shift of dominant failure mode from mode I to mode II was observed, although crack propagation under bending was governed macroscopically by mode I cracking[3].

In the present paper, the two-domain BEM model is applied to solving crack propagation due to rebar corrosion. For early detection of corrosion, non-destructive testing (NDT) is available. It is confirmed that corrosion potential on the reinforcement could be estimated by a compensated improved half-cell potential measurement[4]. This implies that the zone of intense corrosion product is able to be located by NDT. Provided that pressure distribution due to expansion of corrosion products could be assumed, prediction of crack propagation in concrete is readily performed prior to corrosion damage.

In order to develop this integrated procedure for prediction of crack initiation and propagation based on NDT, crack extension in concrete due to corrosion product is studied, on the basis of LEFM and BEM.

Table 1 Dimension of the specimens

Specimen type	Dimension of the specimens	Purpose
Beam	10cmX10cmX40cm	Estimation of stress intensity factors
Slab	25cmX25cmX10cm	Corrosion cracking of rebar
Cylinder	10cm diameter X 20cm height	Mechanical properties of concrete

Table 2 Mixture proportion

Mixture	Weight per unit volume (kg/m^3)				Max. aggregate size (G_{max})
	Water (W)	Cement (C)	Sand (S)	Gravel (G)	
Concrete	172	344	830	1021	20mm

W/C	s/a	Air-entrained admixture	Slump	Air content
50%	48%	104cc	7.3cm	5.5%

2. EXPERIMENTS

Specimens employed are summarized in **Table 1**. Three types of specimens were tested as stated below:

1. Notched beam: Experiments were carried out under 3-point bending by a universal testing machine. For determination of the critical stress intensity factor, K_{IC}, 1-channel acoustic emission (AE) system was employed[3].
2. Slab: Experiments were carried out for simulation of corrosion cracking by expansive agent (using dolomite paste). Two cases of 3cm and 8cm cover thickness were studied
3. Cylinder: Experiments were carried out for determination of mechanical properties of concrete.

(1) Preparation of specimens

The concrete specimens were cured in water for 28days in the standard room (20°C). Mixture proportion and mechanical properties are summarized in **Tables 2** and **3**. Specimens were made of plane concrete. The water cement ratio by weight (W/C) and the volume ratio of fine aggregate (s/a) are common for all specimens. The maximum gravel size is 20mm. To keep the slump value around 7cm by mix, air-entraining admixture was added. Mechanical properties were obtained from cylindrical specimens at the age of 28days. These are given in **Table 3**. Young's modulus and Poisson's ratio are applied to BEM analysis.

Table 3 Mechanical properties

Compressive strength (MPa)	Tensile strength (MPa)	Poisson's ratio	Young's modulus (GPa)	P-wave velocity (m/sec)
37.9	3.03	0.22	29.7	4,730

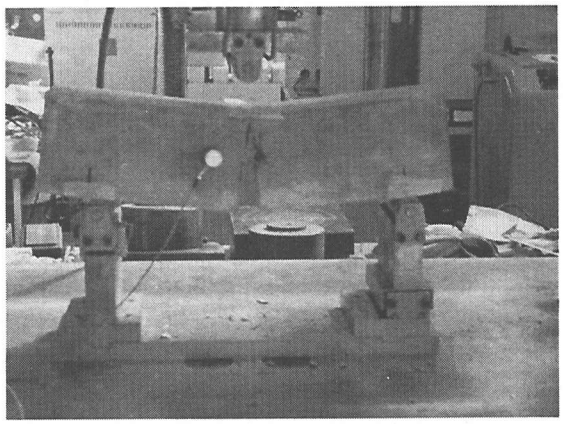

Photo 1 Experiment with 1-channel AE system.

(2) Bending Test

3-point bending test was conducted for the beam specimen. At the age of 28days, notches of 3cm, 5cm and 7cm depths with 1mm width were made by sawing at the center of the specimen. A universal testing machine was employed for loading as shown in **Photo 1**. The load was applied at the top center of the beam and was measured by a load-cell. Loading rate was controlled as 0.01mm/min. Inserting a clip gauge into the notch mouth, the crack-mouth opening displacement (CMOD) was measured. AE sensor employed was of the resonance frequency 150kHz. For the measuring system, the frequency range was from 10kHz to 1MHz and the amplification was 60dB gain in total. AE events under crack propagations were detected, amplified, filtered and recorded by using a LOCAN-TRA system (PAC).

The critical stress intensity factor K_{IC} of concrete was determined from the analysis of AE activity[2]. The averaged K_{IC} values of the three specimens were 0.847MPa $m^{1/2}$, 0.827MPa $m^{1/2}$ and 0.723MPa $m^{1/2}$ for the notch depth 3cm, 5cm and 7cm, respectively. Using the value K_{IC}=0.723MPa $m^{1/2}$ for an input data, crack propagations were analyzed by BEM. This is because the value of K_{IC} was also evaluated from Barenblatt's criterion[2]. Results are shown in **Table 4**. Barenblatt's criterion is given in Eq.(1),

Table 4 Evaluation of the values K_{IC} by Barenblatt's criterion

Notch Depth	K_{IC} (MPa $m^{1/2}$)	Calculated notch depth $(K_{IC}/\sigma_t)^2$	Barenblatt's criterion
3cm	0.847	6.1cm	Not satisfied
5cm	0.827	4.96cm	Just satisfied
7cm	0.723	3.06cm	Fully satisfied

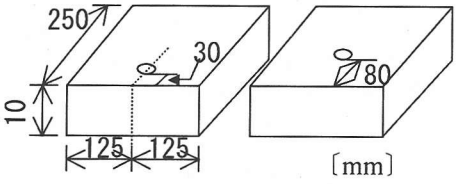

Fig.1 Sketch of the specimens.

$$a \geq \left(\frac{K_{IC}}{\sigma_t} \right)^2 \qquad (1)$$

As can be seen, the specimen of 7cm notch is so fully satisfied with Eq.(1) that the value of K_{IC} of concrete is determined as 0.723MPa $m^{1/2}$.

(3) Simulation of corrosion cracking by expansive agent

Two types of specimen with 3cm and 8cm cover thickness were prepared as shown in **Fig.1**. To simulate corrosion cracking of mixed mode, an expansion test was conducted. Corrosion of the reinforcement takes a long process and it is very difficult to examine in the short time by an experiment. Thus, hydrostatic radial pressure is introduced by employing expansive agent. In **Fig.1**, a circle of 3.0cm diameter represents the location of the reinforcement where the expansion pressure is applied by dolomite paste.

Crack propagation due to the expansion observed for cover thickness 3cm and 8cm are shown in **Figs.2** and **3**. The crack traces for 3cm cover thickness in **Fig.2** are also shown in **Photo 2**.

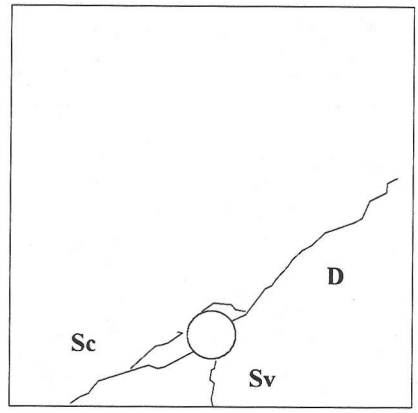

Fig.2 Observed crack patterns (3cm cover thickness).

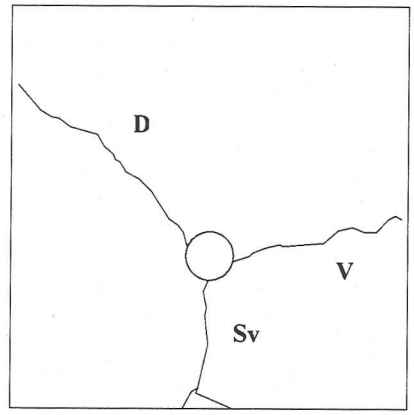

Fig.3 Observed crack patterns (8cm cover thickness).

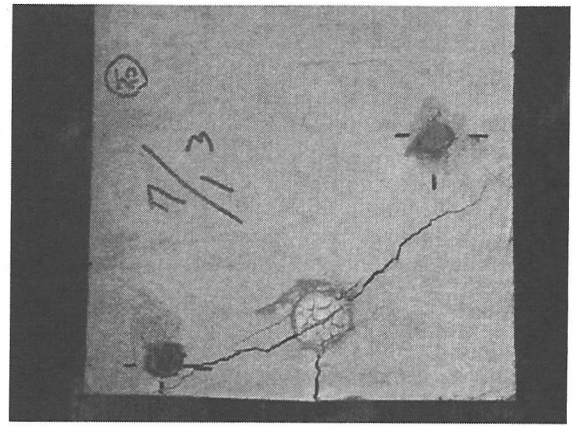

Photo 2 Crack patterns observed for 3cm cover thickness.

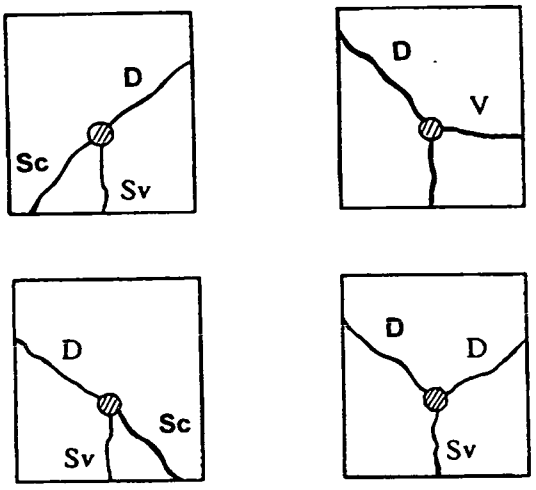

Fig.4 Observed crack patterns due to corrosion

3. OBSERVED CRACK PATTERNS

From the previous study[5], particular crack patterns were identified around the reinforcement. Examples are given in **Fig.4**. Observed crack patterns are classified into four patterns. One is a surface crack, which propagates vertically to the surface in the region of concrete cover. It is marked as 'Sv'. Others are, a spalling crack marked as 'Sc', a vertical crack marked as 'V', and a diagonal crack marked as 'D'.

Because concrete is inhomogeneous, there exit many possibilities for crack initiation and crack propagation. A spalling crack (Sc), a surface crack (Sv), and a diagonal crack (D) are observed in the case of cover thickness 3.0cm in **Fig.2**. In the case cover thickness 8.0cm, a surface crack (Sv), a diagonal crack (D), and a vertical crack (V) are observed in **Fig.3**. The spalling crack could be nucleated in the case of the surface crack being arrested by aggregate[5]. According to the stress analysis, the spalling crack and/or the diagonal crack could follow the surface crack due to hydrostatic expansion of corrosive products[6]. With the increase of lateral expansion, the vertical crack could follow the spalling crack.

From the theory of elasticity, circumferential tensile stress $\sigma_{\theta\theta}$ around a hole which is applied to the interior surface of the hole is given under hydrostatic pressure, p as,

$$\sigma_{\theta\theta}(r) = p[1+(a/r)^2] - p \qquad (2)$$

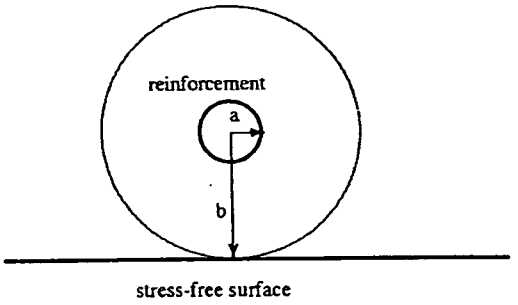

Fig.5 Configuration of reinforcement near the surface.

It is easily realized that the tensile stress reaches the maximum at the surface of the hole (r = a). This leads to a conclusion that a crack could initiate anywhere around the hole under hydrostatic pressure. In an actual condition, there exists a stress-free surface near the reinforcement as shown in **Fig.5**.

In this case, it is possible to approximate stress distribution by taking into account an annular body with the outer diameter, b, as

$$\sigma_{\theta\theta}(r) = p[1+(a/r)^2]/[p - (a/b)^2] - p \qquad (3)$$

At the point on the hole closet to the stress-free surface, in other words, at the point of the shortest cover thickness, the maximum tensile stress is obtained from Eq.(3). Thus the elastic theory offers only one possibility for the initiation of the surface crack 'Sv'. Thus, other cracks than the surface crack could be nucleated either by following the surface crack or in the case of the surface crack 'Sv' being arrested by the aggregate. Taking into account these findings, the cracking mechanisms of the cases shown in **Figs.2** and **3** are investigated analytically by BEM based on LEFM.

4. BEM FORMULATION

The boundary integral equation on traction t(y) and displacement u(y) defined on boundary S is represented as,

$$Cu_i(x) = \int_S [U_{ij}(x,y)t_j(y) - T_{ij}(x,y)u_j(y)]dS \qquad (4)$$

where C is the configuration coefficient and is readily calculated by eliminating rigid body motion. In the case of smooth boundary, $C = 1/2.U_{ij}(x,y)$ and $T_{ij}(x,y)$ are fundamental singular solutions in the two dimensional BEM of elastostatics. For the two-dimensional linear elastic body under plane stress condition, they are given as

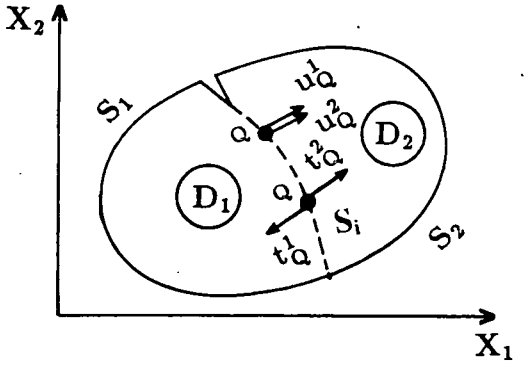

Fig.6 Two-domains for the analysis

$$G_{ij}(x, y) = \frac{2(1+\nu)^2}{8\pi E}\left\{\frac{3-\nu}{1+\nu}\delta_{ij}\log(1/r) + r_{,i}r_{,j}\right\}$$
$$T_{ij}(x, y) = \frac{1}{4\pi r}\left\{[(1-\nu)\delta_{ij} + 2(1+\nu)r_{,i}r_{,j}]\frac{\partial r}{\partial n} - (1-\nu)(r_{,i}n_j - r_{,j}n_i)\right\} \quad (5)$$

where $r = |x - y|$ and the comma denotes the spatial derivative. δ_{ij} is Kronecker's delta, E is Young's modulus, and ν is Poisson's ratio.

Two domains D_1 and D_2 are joined along a common interface S_i as shown in **Fig.6**. S_1 and S_2 represent the external boundaries of D_1 and D_2, respectively. Hence, $S_1 + S_i$ constitutes the boundary of the domain D_1, and $S_2 + S_i$ designates the boundary of D_2. The boundary integral equation for each region is given as similar to Eq.(4)[7]

The boundary conditions are imposed separately on S_1 and S_2, while the compatibility conditions on the interface S_i are given by

$$\begin{cases} u_j^1(Q) = u_j^2(Q) \\ t_j^1(Q) = -t_j^2(Q) \end{cases} \quad (6)$$

with Q denoting any point on S_i.

Discretizing the boundaries of the two domains and the interface boundary, a constant element is adopted for traction and a linear element is assigned for the displacement on the boundary elements[8].

Carrying out the numerical integration over the elements using 6-points Gaussian integration and taking care of the diagonal terms, Eq.(4) is written in the following matrix form for each region α,

$$[H^{\alpha}_{ij}]\{u^{\alpha}_i(y^{\alpha}_i)\} = [G^{\alpha}_{ij}]\{t^{\alpha}_j(y^{\alpha}_i)\} \quad (\alpha=1,2) \quad (7)$$

where the super-script α denotes the two domains.

To mark the numerical scheme comparable with the conventional finite element method (FEM) code, **Eq.(7)** is converted into the equation, not of traction on the element, but of nodal forces, as follows:

$$\{N^{\alpha}_{km}\}[uG^{-1}{}_{ml}(H_{ij})]^{\alpha}\{u^{\alpha}_j\} = \{f^{\alpha}_k\} \quad (\alpha=1,2) \quad (8)$$

where N_{km} is the shape function to obtain nodal forces from tractions. Making use of Eq.(6), the matrix Eq.(8) for (α= 1,2) are coupled together, and thus the resulting equation is solved for the nodal forces and displacements.

5. ANALYTICAL MODEL

Analytical models for mixed-mode fracture of case-1, case-2 and case-3 are shown in **Figs.7**, **8** and **9**. These are case-1 for simulating the spalling crack, case-2 for the surface and vertical cracks, and case-3 for the diagonal crack. Only a half portion of the specimen is considered for the analysis. This is because each crack trace is to be analyzed. Thus, crack generating mechanisms for all the cases are analytically investigated. All boundary meshes are of 5mm long. The effect of mesh sizes and the termination point T on the numerical accuracy was previously studied[3),7),8)]. It is found that the accuracy of solutions is insensitive to the mesh division in the elastic problem. In the case of the two-domain BEM, however, the mesh size of the interfaces should be identical to that of the boundary element, in order to increase the accuracy. Further, the shorter the length of the element becomes, the more distorted the orientation of the crack trace at the interface is. This case was particularly observed when the element length is equal to 1mm. Based on these results, the size of the mesh, 5mm, is selected for all elements in the present analysis.

Because expansive agent was employed in the experiment, pressure distribution of hydrostatic radial pressure is only taken into consideration to simulate the expansion of corrosive products.

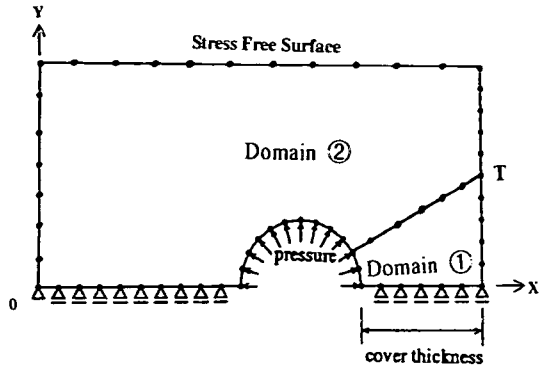

Fig.7 Two-domain BEM model of case-1for simulating the spalling crack (Sc).

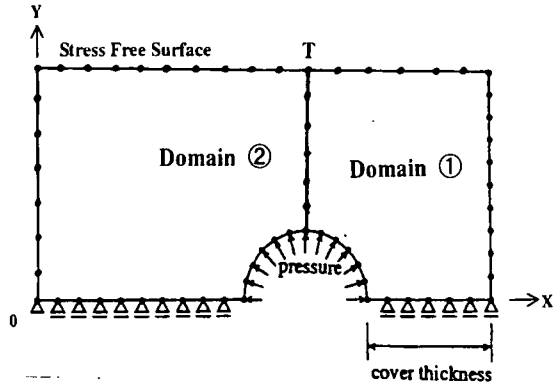

Fig.8 Two-domain BEM model of case-2 for simulating the surface crack (Sv) and the vertical crack (V)

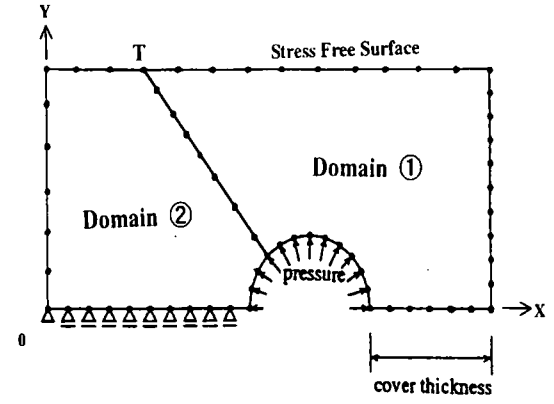

Fig.9 Two-domain BEM model of case-3 for simulating the diagonal crack (D)

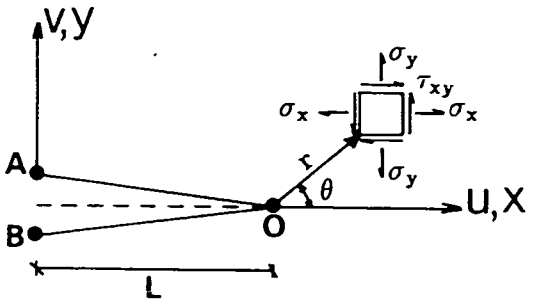

Fig.10 Crack tip elements

It is important to point out one remark concerning selection of common interface. To the best of the authors' knowledge, the original interface has to be taken as close as possible to the plausible final failure surface. In this respect, the straight line joining the crack tip from the crack initiation to the termination T is as close as possible to the crack trace actually observed.

6. CRACK PROPAGATION ANALYSIS

The stress intensity factors at the crack tip are determined by Smith's one-point formulae[9]. K_I and K_{II} are determined from relative displacements of the end nodes A and B on the crack tip elements as shown in **Fig.10**.

The criterion for crack extension to an arbitrary direction is derived from the criterion by Erdogan-Sih, the direction of the maximum tangential stress θ is determined from the relation[10].

$$K_I \sin\theta + K_{II}(3\cos\theta - 1) = 0 \qquad (9)$$

where K_I and K_{II} are the stress intensity factors of mode I and mode II, respectively. Crack nucleation is governed by the following equation,

$$\cos\frac{\theta}{2}\left[K_I \cos^2\left(\frac{\theta}{2}\right) - \frac{3}{2}K_{II}\sin\theta\right] = K_{IC} \qquad (10)$$

When a crack propagates, the node at the crack tip is separated into two nodes, creating a new stress-free crack boundary in the direction θ. Then, a new interface boundary is defined from the new crack tip. The procedure mentioned above is implemented and crack propagation in arbitrary directions can be automatically traced[7].

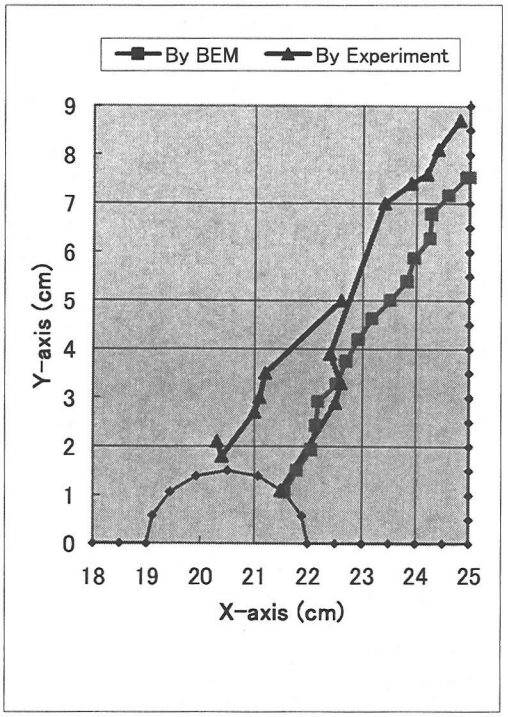

Fig.11 Crack traces of 3cm cover thickness for spalling crack.

In **Figs.7**, **8**, and **9**, a starting crack-tip corresponds to the lower end of the interface boundary. The direction θ of crack extension is determined by Eq.(9). The pressure level corresponding to the critical intensity factor K_{IC} was determined from Eq.(10). Then two crack elements are newly put forth in the direction θ at the crack-tip, generating new interface boundary between the crack-tip and the termination point T in the figures.

7. RESULTS AND DISCUSSION

(1) Case 1: the spalling crack

Crack trace of the spalling crack shows reasonable agreement with that of the actual crack as shown in **Fig.11**. Here-in-after, based on the coordinate systems in **Figs.7, 8** and **9**, only the regions of the crack traces targeted are emphasized and shown. Thus, the abscissas in **Figs.11, 13a, 13b, 15** and **17** denote the coordinates targeted in the X-axis. Because two branches of the crack trace were observed, only one is taken into consideration. From BEM analysis, ratios of stress intensity factors of mode I to mode II are plotted with the increment of crack extension, results are shown in **Fig12**.

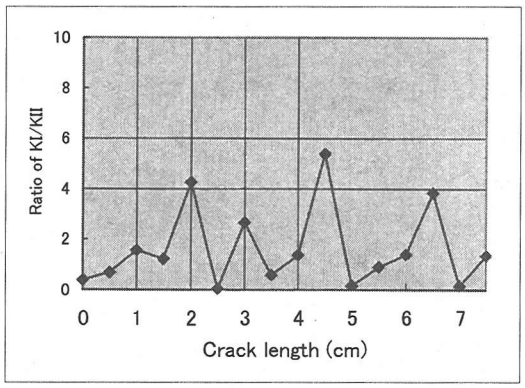

Fig.12 Ratios of stress intensity factors (K_I/K_{II}) for spalling crack.

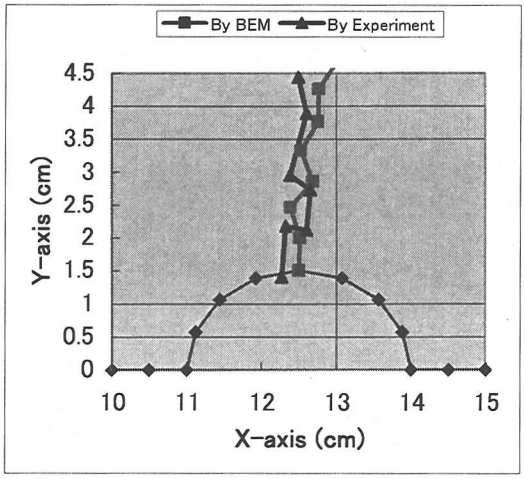

Fig.13a Crack traces of 3cm cover thickness for surface crack.

It is observed that in the beginning of crack extension, the ratio of stress intensity factors (K_I/K_{II}) are less than 1.0 and then higher ratios are observed. This indicates that the crack starts with mixed mode. But crack extension is dominated by the mode-I fracture. The numerical accuracy is so sensitive to the boundary meshes in BEM that minor variations of the stress intensity factors are consequent. This is probably a reason why the crack trace analyzed is not always straight and the ratios of the stress intensity factors are varied irregularity.

(2) Case 2: the surface crack and the vertical crack

Crack trace of the surface cracks simulated for both cases (3cm and 8cm cover thickness) show good agreement with the actual crack as shown in **Fig.13a** and **13b**. The ratios of stress intensity factors of mode I to mode II are plotted with the increment of crack extension in **Fig14**.

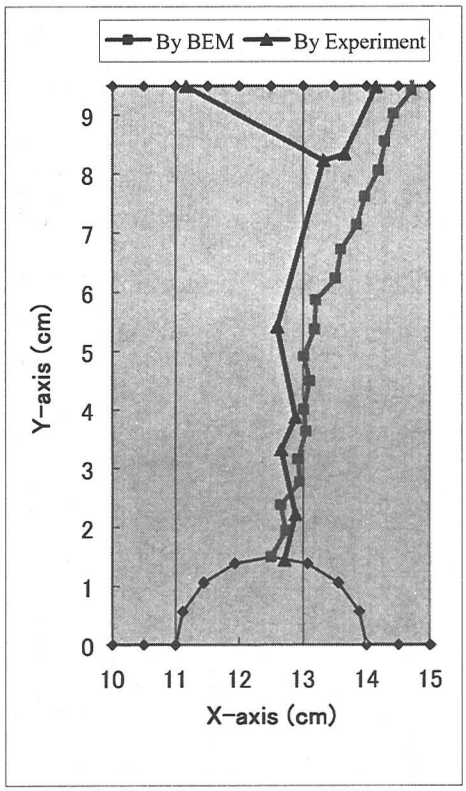

Fig.13b Crack traces of 8cm cover thickness for surface crack.

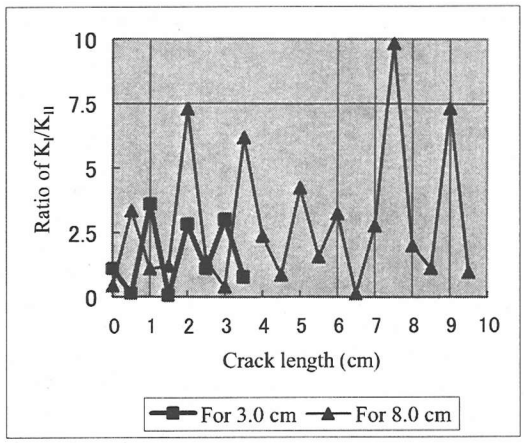

Fig.14 Ratios of stress intensity factors (K_I/K_{II}) for surface cracks.

It is observed again that the ratios of stress intensity factors (K_I/K_{II}) are mostly greater than 1.0 with alternate lower ratios. This result reveals that the mode-I fracture dominates mode-II fracture during propagation of the surface crack.

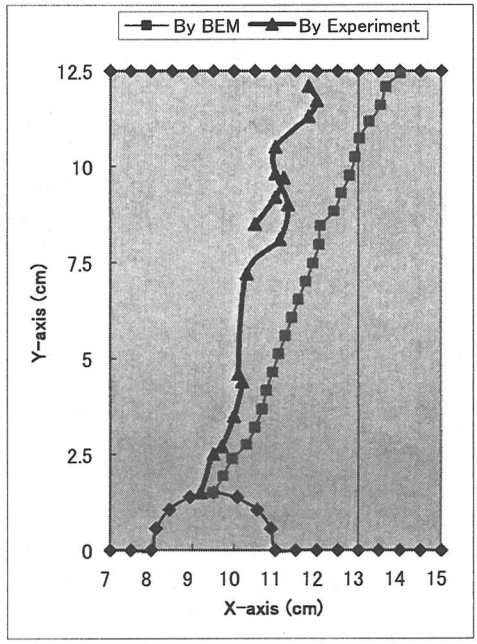

Fig.15 Crack traces of 8cm cover thickness for vertical crack.

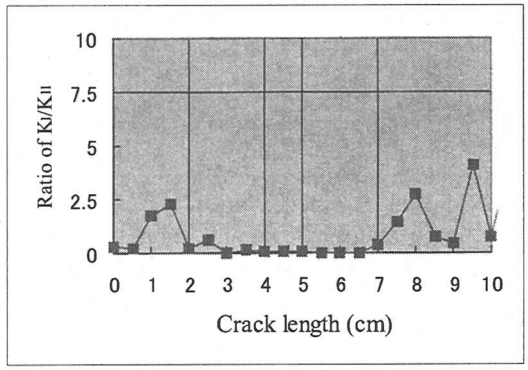

Fig.16 Ratios of stress intensity factors (K_I/K_{II}) for vertical crack.

In **Fig.15**, results of the vertical crack are shown. Again, it shows good agreement with the actual crack. The ratios of stress intensity factors of mode I to mode II are plotted in **Fig.16**.

It is observed that the ratios of stress intensity factors (K_I/K_{II}) are mostly less than 1.0. This indicates that the crack propagates with almost mode-II fracture. Only in the beginning and the final stage, the larger ratios are observed. This result reveals that the mode-II fracture dominates during extension of the vertical crack.

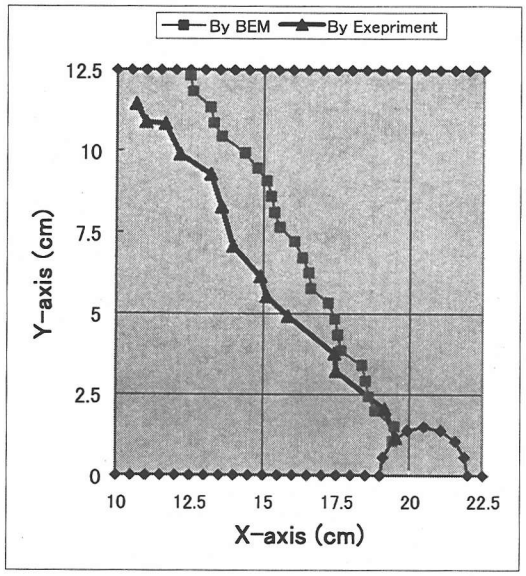

Fig.17 Crack traces of 3cm cover thickness for diagonal crack.

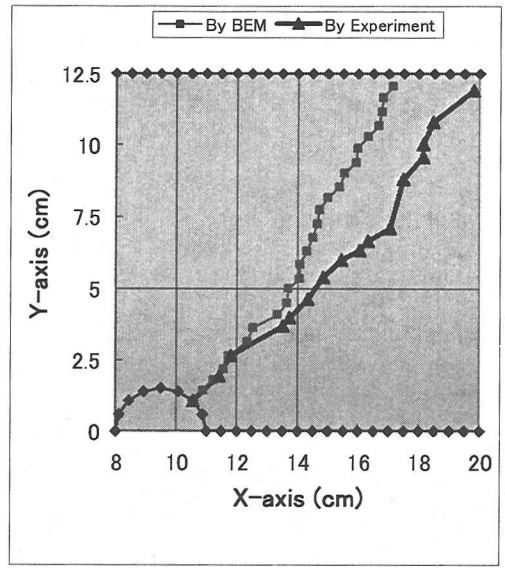

Fig.18 Crack traces of 8cm cover thickness for diagonal crack.

(3) Case 3: the diagonal crack

Crack trace of the diagonal cracks show reasonable agreement with the actual crack as shown in **Figs.17** and **18**.

According to Fig.19, it is observed that the ratios of stress intensity factors (K_I/K_{II}) are greater than 1.0 for 3cm cover thickness and less than 1.0 for 8cm cover thickness. For 3cm cover thickness, the mode-I fracture dominates more than mode-II fracture, while it reverses for 8cm cover thickness. This discrepancy may result from the fact that the diagonal crack of 3.0cm cover thickness extended following the spalling crack, while that of 8.0cm cover thickness followed the vertical crack.

Thus, it is clarified from the analysis that cracks observed due to corrosion are nucleated from different mechanisms.

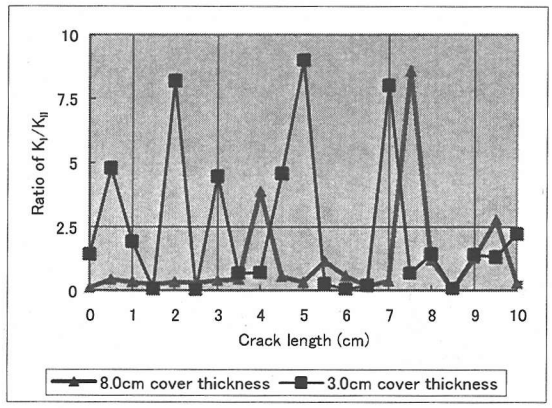

Fig.19 Ratios of stress intensity factors (K_I/K_{II}) for diagonal cracks.

8. CONCLUSION

As a numerical technique, two-domain BEM is very promising for implementing an analysis of the mixed-mode discrete crack extension based on the maximum circumferential stress criterion. The method is readily applicable and allows simple automatic remeshing to model crack extension. Results obtained are summarized, as follows:

(1) By applying the two-domain BEM, corrosion cracking in the arbitrary direction is automatically simulated on the surface crack, the spalling crack, the vertical crack and the diagonal crack.

(2) Because reasonable agreement between the crack trace analyzed and observed in the experiments, cracking mechanisms are investigated by calculating the ratio of stress intensity factors.

(3) From the results, it is clarified that crack patterns observed due to corrosion result from different mechanisms. The surface crack and the spalling crack are mostly governed by mode I failure, while the vertical crack and the diagonal crack could be nucleated due to mode II failure.

ACKNOWLEDGEMENT: The authors wish to thank Assoc. Professor M. Shigeishi, faculty technician Mr. Y. Tomoda and graduate student Mr. K. Ishiharaguchi in Kumamoto University for their collaboration during the experiment and analysis.

REFERENCES

1) Matsushima, M., Tsutumi, T., Seki, H., and Matsui, K.: Design of Cover Thickness for Reinforced Concrete Structures Subjected to Sever Salt Attack, Proc. of JSCE, No. 490/V-23, pp.41-49, 1994 (in Japanese)
2) Farid Uddin, A.K.M., Ishiharaguchi, K. and Ohtsu, M,: Stress Intensity Factors by Acoustic Emission and Analysis of Crack Propagation by Boundary Element Method, Proceeding of the 15th International AE Symposium, Progress in AE X, pp.11-16, 2000.9
3) Chahrour, A.H. and Ohtsu, M.: Crack Growth Prediction in Scaled Down Model of Concrete Gravity Dam, Theoretical and Applied Fracture Mechanics, 21, pp. 29-40, 1994
4) Ohtsu, M. and Yamamoto, T.: Compensated Procedure for Half-Cell Potential Measurement, Construction and Building Materials, Vol. 11, Nos. 7-8, pp.398-402, 1997.12
5) Ohtsu, M. and Yoshimura, S.: Analysis of Crack Propagation and Crack Initiation due to Corrosion of Reinforcement, Construction and Building Materials, Vol. 11, Nos. 7-8, pp.437-442, 1997.12
6) Ohtsu, M., Tutumi, T., Murakami, Y., and Kudo, Y.: Analytical and Experimental Study on Crack Propagation due to Rebar Corrosion, Proc. Japan Concrete Institute, 17(1), pp.955-960, 1995 (in Japanese)
7) Chahrour, A.H., and Ohtsu, M.: Multi-Domain BEM Implementation for Mixed-Mode Cracking in Concrete, Fracture and Damage of Concrete and Rock, FDCR-2, E & FN Spon, London, pp.196-205, 1992
8) Chahrour, A.H., Fukuchi, S., Ohtsu, M. and Tomoda, Y.: BEM Analysis of Mixed-Mode Crack Propagation in Center-Notched Concrete Beams, Transactions of JCI, Vol.15, pp. 201-208,1993.12
9) Smith, R.N.L. and Mason, J.C.: A Boundary Element Method for Curved Crack Problems in Two Dimensions, Boundary Element Methods in Engineering, Springer-Verlag, Berlin, pp.472-484, 1982
10) Erdogan, F. and Sih, G.C.: On the Crack Extension in Plates under Plane Loading and Transverse Shear, J. Basic Eng., No.12, pp.519-527, 1963.12

(Received April 26, 2001)

鉄筋腐食による混合モードひび割れ進展の BEM 解析

Farid UDDIN A. K. M.・大津政康

鉄筋腐食の発生により，コンクリート中にはひび割れが発生する．そのひび割れパターンについて実験的並びに解析的に研究を行った．鉄筋周囲に発生する様々なひび割れパターンに注目し，その発生・進展機構を境界要素法（BEM）を用いて解析により明らかにした．解析では混合モードひび割れを取り扱うために，線形破壊力学の最大周方向応力基準に基づき二領域 BEM 解析コードを用いて，膨張剤を用いた実験で観察された表面ひび割れ，内部ひび割れの進展機構を検討し，それらの卓越破壊モードが異なることを明らかにした．